Materials Today Bio 29 (2024) 101376

Contents lists available at ScienceDirect

Materials Today Bio

journal homepage: www.journals.elsevier.com/materials-today-bio

Enhanced sclerotherapy for vascular malformations: A dual-mechanism approach using in-situ forming PATDs gel

Jizhuang Ma [a,b], Wenhan Li [c], Yu Ding [a], Yongfeng Chen [a], Xiaoyu Huang [a], Tong Yu [a], Di Song [a], Haoran Niu [a], Bao Li [a], Huichao Xie [b], Keda Zhang [b], Tianzhi Yang [d], Xiaoyun Zhao [e], Xinggang Yang [a,*], Pingtian Ding [b,a,**]

[a] School of Pharmacy, Shenyang Pharmaceutical University, Shenyang, 110016, China
[b] College of Pharmacy, Shenzhen Technology University, Shenzhen, 518118, China
[c] Ultrasound Department, Shengjing Hospital, China Medical University, Shenyang, China
[d] Department of Basic Pharmaceutical Sciences, School of Pharmacy, Husson University, Bangor, ME, USA
[e] School of Life Science and Biopharmaceutics, Shenyang Pharmaceutical University, Shenyang, 110016, China

ARTICLE INFO

Keywords:
Vascular malformations
Sclerotherapy
Tranexamic acid
Polyoxyethylene alkylether tranexamate derivatives
Plasmin
Low-molecular-weight hydrogel

ABSTRACT

Vascular malformations are common vascular lesions in infants and seriously affect their health and quality of life. Vascular sclerotherapy is an effective treatment for vascular malformations. However, current sclerosants have difficulty achieving both high efficiency and low toxicity, and their dosing forms make it difficult to achieve long-term retention in the affected blood vessels. Therefore, exploring a safe and effective sclerosant and its delivery strategy is the key to clinical sclerotherapy. To address the above issues, this study developed sclerosants that could form an in-situ gel based on a dual mechanism of vascular injury and plasmin (PLA) inhibition. By linking the non-ionic surfactant sclerosant polyoxyethylene alkyl ether (PAs) and the PLA inhibitor tranexamic acid (TA) through an ester bond, a cationic surfactant sclerosant polyoxyethylene alkylether tranexamate derivatives (PATDs) were constructed. The cationic charge of PATDs enhanced its cytotoxicity to HUVEC-TIE2-L914F cells, and the ester bond of PATDs could be degraded by esterase in the blood, reducing its systemic toxicity. The degradation product TA inhibited the activation of the PLA-matrix metalloproteinase (MMPs) system induced by vascular injury, thereby promoting the deposition of collagen and the proliferation and differentiation of fibroblasts to promote vascular fibrosis. In addition, an injectable solution (PATDs/GA) was prepared by mixing PATDs with glycerol formaldehyde (GA), and PATDs/GA could form a low-molecular-weight gel automatically in an aqueous solution, which was beneficial to increase its retention in the affected blood vessels and reduce the risk of drug entering non-targeted sites. At the same time, this gel automatically dissolved, reducing the risk of immune rejection caused by long-term retention. This study provided a new and precise approach for the treatment of vascular sclerosis with high efficiency and low toxicity.

1. Introduction

Venous malformation, the most common type of vascular malformation, can occur in any anatomical site or tissue. It is most commonly seen in the head and neck region of infants, significantly affecting their aesthetic appearance [1,2]. Pain is the most frequent symptom associated with venous malformations, and in advanced stages, spontaneous bleeding may occur [3]. Currently, treatment options for venous malformations include vascular sclerotherapy, laser irradiation, and surgical excision [4,5]. Among these options, the preferred approach for most clinicians is the direct injection of a sclerosant into the lesion [6,7].

The principle of vascular sclerosis treatment involves injecting sclerosants into the affected blood vessels. These agents cause cellular damage to the vascular endothelium, disrupting the integrity of the abnormal blood vessels and leading to a process of vascular fibrosis. Eventually, the abnormal blood vessels disappear completely and are replaced by fibrous tissue [8]. Commonly used sclerosants in clinical include absolute ethanol, and detergent-based sclerosants, such as

* Corresponding author. School of Pharmacy, Shenyang Pharmaceutical University, Shenyang, 110016, China.
** Corresponding author. College of Pharmacy, Shenzhen Technology University, Shenzhen, 518118, China.
E-mail addresses: yangxg123@163.com (X. Yang), dingpingtian@sztu.edu.cn (P. Ding).

https://doi.org/10.1016/j.mtbio.2024.101376
Received 11 September 2024; Received in revised form 13 November 2024; Accepted 29 November 2024
Available online 30 November 2024

polidocanol (POL), sodium tetradecyl sulfate (STS), etc [6]. Furthermore, various innovative formulations have been developed to improve the efficacy of sclerotherapy [9–11]. For example, Kathleen and others studied gold nanoparticles for the photothermal therapy of venous malformation [12]. However, photothermal therapy exhibits limitations, particularly concerning its penetration depth, which consequently restricts its efficacy in treating venous malformations [13]. Another approach is the use of gel formulations as a delivery system for sclerosants [14–18]. Fatemeh and others utilized chitosan thermosensitive hydrogel as a carrier for the delivery of doxycycline to treat vascular malformations [16]. However, a limitation of this formulation is the difficulties associated with the degradation of high molecular weight material, which may lead to a localized skin necrosis reaction.

The currently used sclerosants have some limitations [9]. Firstly, there is an imbalance between their therapeutic efficacy and toxicity. Sclerosants like absolute ethanol and bleomycin have strong treatment effects but also induce significant toxic side effects [19,20]. On the contrary, detergent-based sclerosants have milder effects but may lead to lower treatment efficacy [21]. Secondly, the current sclerosants only focus on damaging the vascular endothelial cells without intervening in the process of vascular fibrosis [22]. After endothelial cell injury, thrombus formation may occur, leading to activation of the plasmin (PLA)-matrix metalloproteinase (MMPs) system [23–25]. Studies have reported that the PLA-MMPs system can induce the degradation of

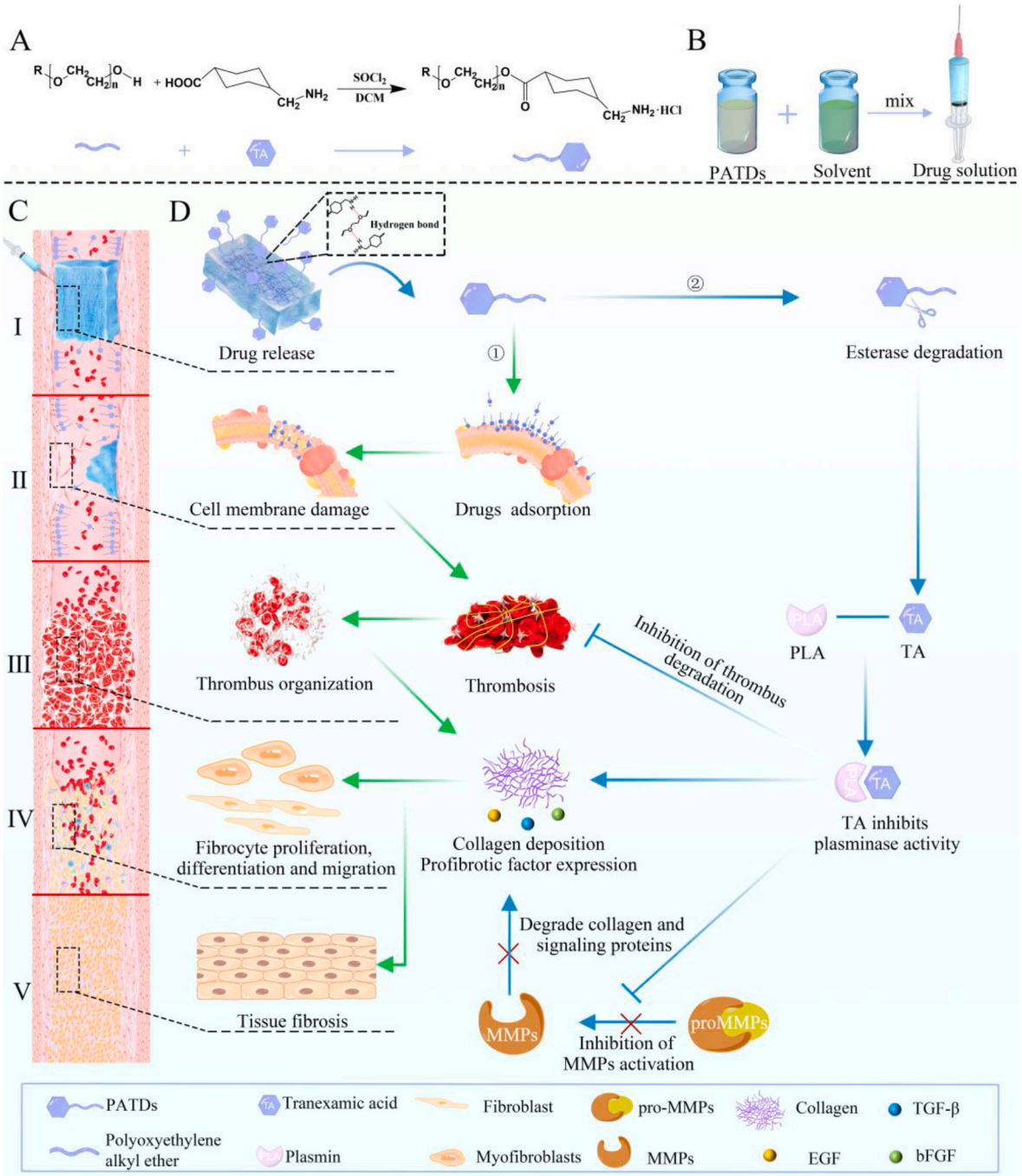

Scheme 1. (A) PATDs synthesis route. (B) PATDs/GA solution preparation. (C) Vascular sclerosing process illustration of PATDs in-site gel sclerotherapy (I. injection of PATDs/GA solution preparation to form in-site gel, II. vascular damage, III. thrombosis, IV. formation of tissue fibrosis microenvironment, V. vascular fibrosis). (D) "vascular damage-fibrinolytic system inhibition" dual mechanism of vascular sclerosis.

collagen, which is necessary for the process of vascular fibrosis, resulting in incomplete fibrosis and potential complications such as vessel recanalization [26]. Thirdly, due to the location of the lesions within the blood vessels, when these sclerosants are administered as solutions, they get diluted and rapidly cleared by blood flow, making it difficult to achieve optimal treatment effects [27].

To tackle the aforementioned challenges, we have developed a novel cationic surfactant agent (Polyoxyethylene Alkylether Tranexamate Derivatives, PATDs) for the treatment of vascular malformations by conjugating the hydroxyl groups of non-ionic surfactant polyoxyethylene alkyl ether serial compound (PAs) with the carboxyl groups of the PLA inhibitor tranexamic acid (TA) through ester bonds (Scheme 1). The PAs that belong to non-ionic surfactants are clinically used for vascular malformation treatment, but their efficacy is limited due to their mild effect [28]. TA, which is a PLA inhibitor [29], contains both carboxyl and amino groups in its molecular structure and can be used to synthesize a cationic surfactant agent, following the connection of TA with the non-ionic surfactant PAs through ester bonds (Scheme 1A). In addition, an injectable solution (PATDs/GA) was prepared by mixing PATDs with glycerol formaldehyde (GA) which is an organic solvent for drug injections. PATDs/GA could spontaneously crosslink and form a low-molecular-weight gel in an aqueous solution due to their hydrophilic and hydrophobic long chains, which promoted drug retention in the lesion vessels. In an aqueous solution, hydrogen bonds are formed between hydrogen ions at the end of the molecular structure of the material and the electron pairs of polar oxygen atoms, and the alkyl chain fragments are associated through hydrophobic interaction, leading to the formation of gel networks. More importantly, the gel formed by this small molecule compound could dissolve spontaneously under the competition of hydrogen bond forces of water molecules, thereby avoiding immune rejection reactions (Scheme 1B and C). The cationic surfactant PATDs could cause cellular damage to the vascular endothelium, disrupting the integrity of the abnormal blood vessels and leading to the formation of thrombus and vascular fibrosis (Scheme 1D, green arrows). Furthermore, the ester bond of PATDs would be degraded by esterase, and the degradation product TA could inhibit the activation of the PLA-MMPs system after the vascular injury, which would improve the process of vascular fibrosis (Scheme 1D, blue arrows). What's more, the degradation of ester bonds would ensure that it would not cause a risk of systemic toxicity. In summary, we have constructed a cationic surfactant PATD, which was used for sclerotherapy treatment based on its dual effect on vascular damage-PLA system inhibition. What's more, PATDs were developed as an injectable in situ gel formulation to improve drug retention time in lesion vessels.

2. Experimental methods

2.1. Synthesis and characterization of PATDs

TA (6 mmol) was added into a 500 mL three-neck flask, and dichloromethane (200 mL) was added as a solvent. The reaction system was cooled under an ice bath for 30 min. Sulfoxide chloride (7.2 mmol) was slowly added under an ice bath, and the reaction was continued for 12 h at 25 °C. Next, PA3, PA5, PA7, PA9, PA12, and PA15 (8.4 mmol) were slowly added, respectively, and continued to react at room temperature for 24 h. Subsequently, the dichloromethane was removed under reduced pressure, and the product was collected. The crude product was finally purified by silica column chromatography eluting with dichloromethane/methanol, filtered under pressure, dried overnight under vacuum, and the purified product was obtained. PATDs were then characterized by a Fourier transform infrared (FT-IR) and a nuclear magnetic resonance (NMR). FT-IR spectra were recorded in the range between 4000 and 400 cm^{-1} on an FT-IR spectrophotometer (Thermo Nicolet, Madison, Wisconsin). The ^{1}H NMR spectra of PATDs were measured using an NMR spectrometer (Bruker AV-400, Karlsruhe Germany) with D_2O as a solvent.

2.2. Preparation of PATD gel

An appropriate amount of PATDs was added to GA and stirred until dissolved to prepare injectable PATDs/GA solution (0.3 M). The PATDs/GA solution was injected with puncturable properties into a saline solution and observed whether the sample solidified. A needle puncture test was used to identify a formulation with injectable and puncturable properties. To measure injection forces, a compression load cell (iLoad Mini, Loadstar Sensors) was attached to the syringe pump between the driver and the syringe plunger. Steady-state injection forces were measured and converted to pressure using the bore diameter of the syringe (4.8 mm).

2.3. Cytotoxicity test

HUVEC-TIE2-L914F cells (4×10^3 cells per well) were grown overnight in 96-well plates and incubated with different concentrations of PATDs for another 12 h. After the cells were changed with new culture media, 10 μL of CCK-8 solution was added to each well and incubated for 2 h. The absorbance of the mixture in each well was then measured at 450 nm wavelength. Subsequently, cell apoptosis was determined according to the instructions of the Cell Apoptosis Kit. Briefly, HUVEC-TIE2-L914F cells (1×10^6 cells per well) were grown overnight in 6-well plates and incubated with PATDs (120 μM) for another 12 h. Cells were collected and resuspended by phosphate buffer solution (PBS), stained with Annexin V-FITC and PI at room temperature for 15 min, and the cell apoptosis was determined within 1 h by a flow cytometer.

2.4. Evaluation of embolus in mouse tail vein

Kunming mice were divided into the saline group, POL/GA preparation group, PAs/GA and PATDs/GA preparation group (n = 6). The veins of mice were photographed under an irradiation of 0.5 W light emitting diode (LED) yellow light every 24 h after the administration of treatments. Afterward, blood samples were collected from mouse orbits and cells were separated by a Percoll density gradient centrifugation method as previously described after 24 h administration. The upper layer cells were collected and circulating endothelial cells (CECs) were counted under a microscope.

2.5. Evaluation of embolus in rabbit ear marginal vein

The ear vein of healthy New Zealand rabbits was selected as the therapeutic vessel model, and the experimental animals were divided into the TA group, PA15/GA group, and PATD15/GA group. The blood vessels were photographed and observed every day after the administration of treatments. The embolization length of the treatment vessels and the time for the emboli to disappear in the treatment vessels were measured to evaluate the sclerosing effect.

3. Results

3.1. Computer molecular simulation

This study aimed to enhance the cytotoxicity of the non-ionic surfactant PAs by linking their hydroxyl group with the carboxyl group of the PLA inhibitor TA to design the cationic surfactant PATDs. Simultaneously, under the degradation of esterase, the cationic surfactant PATDs could be degraded and released TA, inhibiting PLA activity and promoting the process of vascular fibrosis. Initially, we utilized computer-aided drug design to examine the electrostatic potential distribution of the compound PATDs, and the results were shown in Fig. 1A, where the red color indicated positive potential, and the blue color indicated negative potential. From the results, it was evident that the electrostatic potential of TA was neutral due to the formation of an

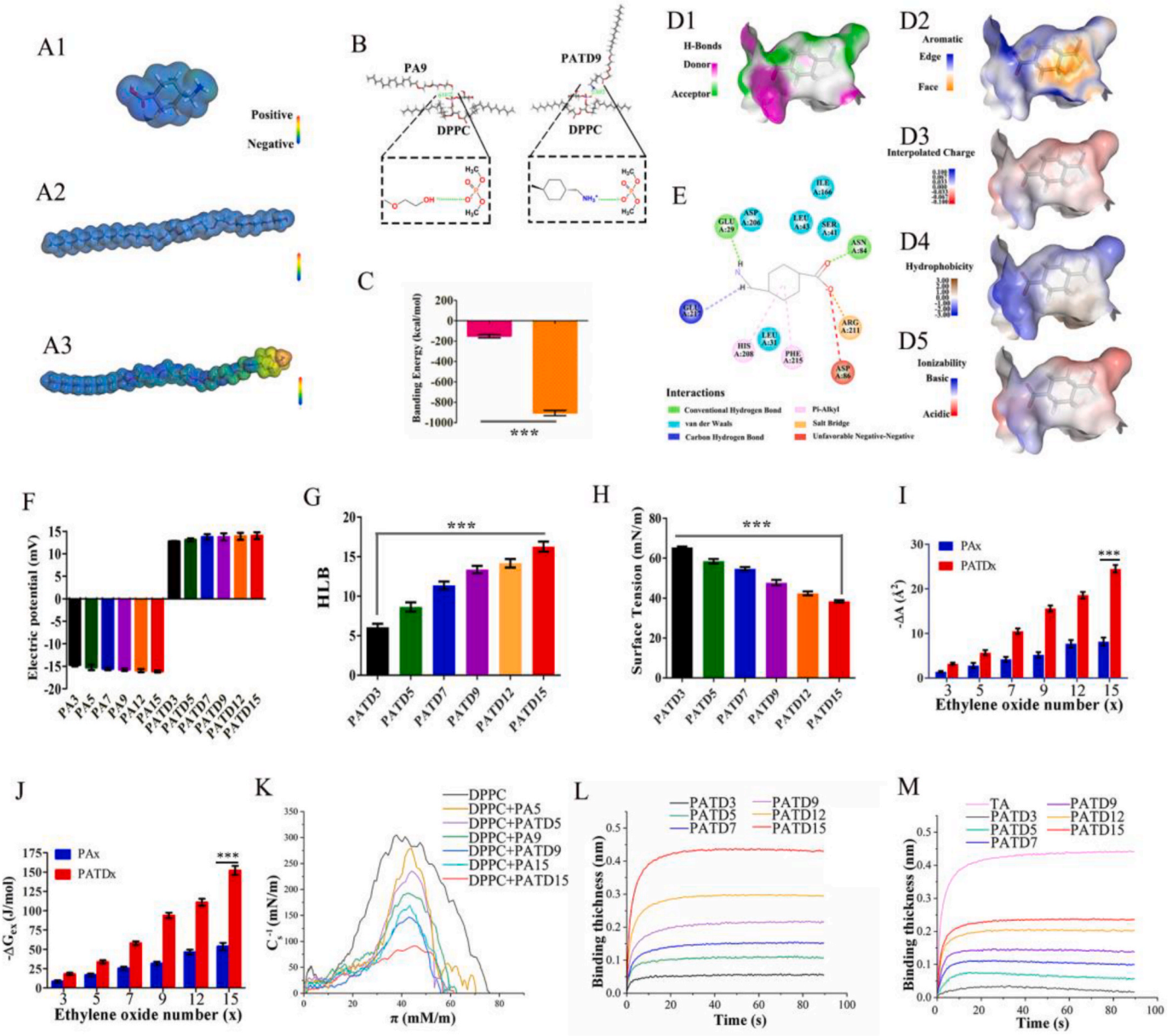

Fig. 1. The potential energy distribution of compound simulations in materials studio. (A1) TA, (A2) PA, (A3) PATD. (B) and (C) Bending energy between PA or PATD and DPPC. The interaction between TA and PLA simulations using Discovery Studio in a 2D view (D1-D5) and 3D view (E). (F) Electric potential of PAs and PATDs. (G) HLB value of PATDs. (H) Surface tension of PATDs. (I) Excess intermolecular distance of mixture of DPPC and PAs or PATDs, x = the ethylene oxide number of the PA or PATD hydrophilic chain. (J) Excess Gibbs energy of mixture of DPPC and PAs or PATDs. (K) Compressibility modulus Cs^{-1} of pure DPPC monolayers, and mixtures of DPPC and PAs or PATDs. (L)Binding curve of PATDs with esterase. (M) Binding curve of TA and PATDs with PLA.

internal salt form between its amino and carboxyl groups. The non-ionic surfactant PAs possessed a slightly negative electrostatic potential. However, the PATDs exhibited a distinct positive potential in one section, indicating they belonged to cationic surfactants. This positive potential facilitated the interaction between the PATDs and the negatively charged cell membrane. Subsequently, we employed Materials Studio analysis software to examine the interaction forces between PATDs and the phospholipid component 1,2-Dipalmitoyl-sn-glycero-3-phosphorylcholine (DPPC) of the cell membrane, and the results were illustrated in Fig. 1B. The interaction between PAs and DPPC was mainly through hydrogen bonding, while that between PATDs and DPPC mainly occurred via ionic bonding. Furthermore, compared to PAs, the binding energy between PATDs and DPPC was significantly lower (Fig. 1C). This suggested that the positive potential of the cation promoted the binding interaction between PATDs and the negatively charged cell membrane.

By employing Discovery Studio analysis software, we investigated the interaction between the TA and PLA. The results, as displayed in Fig. 1D and E, indicated that TA could form in various intermolecular interactions with the PLA, including hydrogen bonding, ionic bonding, hydrophobic forces, etc. This suggested that TA might possess significant inhibitory effects on PLA activity. Based on the aforementioned results, it could be inferred that the PATDs constructed by linking PAs and TA through an ester bond could enhance the cytotoxicity of the compound and potentially exhibit PLA inhibitory effects.

3.2. Synthesis and characterization of PATDs

In order to screen the PATDs with the best sclerosing effect on vascular treatment, we selected six kinds of PAs with hydrophobic chains consisting of straight-chain alkanes with 12 carbons and

hydrophilic chains formed by the polymerization of 3, 5, 7, 9, 12, and 15 ethylene oxide units to connect with TA by esterification for constructing a series of PATDs with gradually increasing hydrophilicity. The synthesized PATDs were characterized by Fourier Transform Infrared (FT-IR) and nuclear magnetic resonance (NMR). In the ^{1}H NMR spectra, the characteristic peaks at 4.19 ppm and 2.81 ppm corresponded to the -COOCH$_2$- and -CH2NH2 in the PATDs, respectively. In the FT-IR spectra, the characteristic peak at 1750 cm^{-1} corresponded to the ester bond in the PATDs. These results showed that the PATDs were successfully prepared (Figs. S1–S3). Furthermore, the analysis of the charge of the PAs and PATDs was measured by the Malvern (Fig. 1F). The results showed that the PAs without TA were negatively charged with a value of around −12 mV, while the charge of the PATDs turned positive with an approximate value of 15 mV after the connection of TA. This indicated that the compounds transformed from non-ionic surfactants into cationic surfactants. Subsequently, the HLB values and surface tension values of the PATDs in aqueous solution were measured. The results showed that the HLB values of PATDs increased gradually from 5 to around 15 with the increase of the length of hydrophilic chains of the PATDs (Fig. 1G), and the surface tension of the PATDs gradually decreased from 64 to 48 mN/m (Fig. 1H), indicating that the ability to decrease the surface tension of the PATDs enhanced gradually with the increase of the length of hydrophilic chains. To investigate whether PATD has the ability of cell membrane damage, the interaction between surfactants and DPPC was investigated by determining the Langmuir-Blodgett membrane of the monolayer formed at the air-water interface of different surfactant/DPPC binary systems. The results showed that both PAs and PATDs could interact with DPPC and decrease the intermolecular distance and Gibbs free energy (Fig. 1I and J). Moreover, compared with the PAs, the interaction force between the PATDs and DPPC was significantly stronger, and the interaction between surfactants and DPPC became stronger with the increase of the hydrophilic chains of the PATDs. The results suggest that as the hydrophilic chain of the compound increases in length, it becomes more prone to stretching in aqueous solutions and binding to the phosphate group of DPPC. Furthermore, the effect of PAs and PATDs on the elastic properties of DPPC phospholipid membranes was calculated (Fig. 1K). The results showed that compared with the PAs, the PATDs could more significantly decrease the elastic properties of DPPC phospholipid membranes, and the ability to decrease the elastic properties increased with the increase of the hydrophilic chains of the PATDs. This indicated that the addition of surfactants could damage the membrane stability of the phospholipid, and the cationic surfactants had a stronger ability to decrease the elastic properties of the membrane. In addition, the interaction between the PATDs and esterase or PLA was also determined by a molecular interaction instrument. The results showed that the interaction between the PATDs and esterase became stronger with the increase of the hydrophilic chains, which indicated that the increase of the hydrophilic chains was advantageous for the exposure of ester bonds and the interaction with esterase (Fig. 1L). In addition, the interaction between the PATDs and PLA was weakened compared with TA (Fig. 1M), but we speculated that the presence of esterase was conducive to the release of TA from PATDs to inhibit the activity of PLA. Based on the above results, PATDs had the potential to damage phospholipid membranes and inhibit the activity of PLA.

3.3. Preparation and characterization of PATD gel

In this study, GA, an injectable organic solvent, was chosen as a dilution agent. The PATDs were mixed with GA to prepare an injectable solution (PATDs/GA), and we injected the PATDs/GA solution into a saline solution to observe whether the sample could solidify. Firstly, the injection pressures were measured to confirm the injectability of PATDs/GA (Fig. S4). Subsequently, it was found that PATD3 and PATD5 had strong hydrophobicity and could not form a gel when in contact with saline, whereas PATD7, PATD9, PATD12, and PATD15 could form a gel when in contact with saline (Fig. 2A). By measuring the viscosity of the PATDs using a rheometer (Fig. 2B), the viscosity values obtained for PATD3, PATD5, PATD7, PATD9, PATD12, and PATD15 were 5.7, 3.4, 2.7, 2.2, 1.8 and 1.6 Pa s, respectively. It was found that the viscosity of PATDs decreased gradually as the length of the hydrophilic chain increased. The viscosity of PATDs gel was measured using a rheometer, and the results (Fig. 2C) showed that the viscosity of PATD7 gel, PATD9 gel, PATD12 gel, and PATD15 gel was 1320, 2750, 2980, and 3375 Pa s, respectively. Compared with the viscosity of the raw materials of PATDs, the viscosity of the PATDs gel was significantly higher and increased with the increase in the hydrophilic chain of the PATDs. Subsequently, the viscoelasticity of PATD7 gel, PATD9 gel, PATD12 gel, and PATD15 gel was studied by using a rheometer (Fig. 2D and E). During the whole frequency range, G′ of these gels was always higher than G″, which strongly proved the solid-like elasticity of the hydrogel characteristic. It was worth noting that G' of the PATD15 gel was greater than those of other hydrogels in both strain scanning and frequency scanning, indicating that it had a greater cross-linking density.

Observation of the microstructure of PATD7 gel, PATD9 gel, PATD12 gel and PATD15 gel by cryogenic electron microscopy (Fig. 2F) revealed that PATD7 gel and PATD9 gel had larger pores on the surface of the gel, while PATD12 gel and PATD15 gel had smaller pores, indicating that as the length of hydrophilic chains increased, the degree of molecular cross-linking increased, resulting in a greater cross-linking density. Subsequently, the erosion rate of PATD7 gel, PATD9 gel, PATD12 gel, and PATD15 gel was examined, with results presented in Fig. 2G. Within the first 5 min, PATD7 gel and PATD9 gel released more than 35 % of the drug, exhibiting severe burst release. This suggested that the gels formed by PATD7 and PATD9 were unstable, and upon initial contact with an aqueous solution, they rapidly dissolved and released drug molecules due to the diffusion of GA. On the other hand, PATD12 gel and PATD15 gel released less than 10 % of the drug within 5 min, indicating that they were capable of forming more stable gels upon contact with an aqueous solution. The low level of burst release reduced the risk of large amounts of drugs entering non-targeted tissues upon initial administration in blood vessels. In addition, PATD7 gel and PATD9 gel were completely dissolved within 60 min, while PATD15 gel dissolved relatively slowly, with complete solubility observed after approximately 120 min. The adhesion of these PATDs gel to tissues was investigated through tissue adhesion experiments, and the results (Fig. 2H) showed that they had certain tissue adhesion abilities, with adhesion values of 300, 360, 520, and 560 N/m^2 for PATD7 gel, PATD9 gel, PATD12 gel, and PATD15 gel. Therefore, they had potential as an intravascular injection material for the treatment of vascular sclerosis. Besides, the gel property of PA7-15 gel was similar to PATD7-15 gel, and the results were shown in Figs. S6–S9. Based on the above results, PA7-15/GA and PATD7-15/GA were injectable and exhibited the property of forming gels upon contact with saline, and the gel strength increased with the growth of the length of hydrophilic chains. What's more, PATD15 gel exhibited a low level of initial burst released, and the formed gel gradually dissolved over time.

3.4. Cytotoxicity and cytotoxic mechanism in vitro

We employed the CCK-8 assay to investigate the cytotoxicity of PAs and PATDs on venous malformation endothelial cells (HUVEC-TIE2-L914F cells), and the results were shown in Fig. 3A and B. As the length of the hydrophilic chain of the PAs and PATDs increased, the surfactants' cytotoxicity against HUVEC-TIE2-L914F cells was significantly enhanced. Furthermore, PAs demonstrated strong toxicity against HUVEC-TIE2-L914F cells at a concentration of 240 μM, while PATDs displayed potent toxicity against HUVEC-TIE2-L914F cells at a concentration of 80 μM. Therefore, PATDs exhibited significantly higher cytotoxicity towards HUVEC-TIE2-L914F cells than PAs. Subsequently, we evaluated the mechanism underlying PATD cytotoxicity against HUVEC-TIE2-L914F cells. Firstly, through lactate dehydrogenase (LDH) release assay (Fig. 3C) and flow cytometry apoptosis assay (Fig. 3E), it

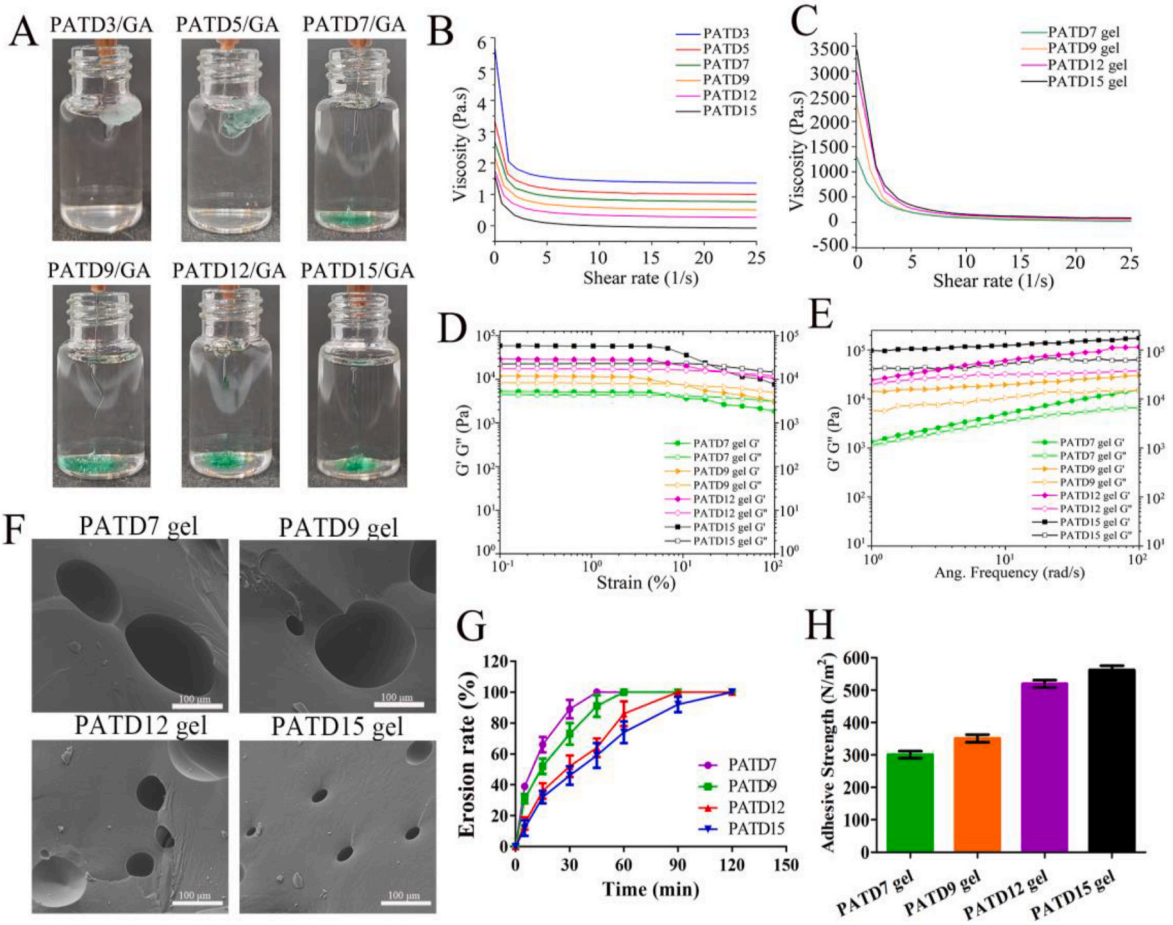

Fig. 2. (A) Macroscopic observation of PATDs gel formation when inject 0.3 M PATDs/GA solution containing green dye into saline. (B) Viscosity of PATD3, PATD5, PATD7, PATD9, PATD12, and PATD15. (C) Viscosity of PATD7 gel, PATD9 gel, PATD12 gel, and PATD15 gel. (D) G′ and G″ of the PATD7 gel, PATD9 gel, PATD12 gel, and PATD15 gel on strain sweep. (E) G′ and G″ of the PATD7 gel, PATD9 gel, PATD12 gel, and PATD15 gel on frequency sweep. (F) Cryoscanning electron microscope image of PATD7 gel, PATD9 gel, PATD12 gel, and PATD15 gel. (G) Erosion behaviors of the PATD7 gel, PATD9 gel, PATD12 gel, and PATD15 gel (n = 3). (H) Adhesive strength of the PATD7 gel, PATD9 gel, PATD12 gel, and PATD15 gel on porcine skin.

could be found that PATDs led to the release of LDH and the cell apoptosis showed a trend consistent with their CCK-8 cytotoxicity result, indicating that its damage to HUVEC-TIE2-L914F cells was partly attributable to its destructive effect on the cell membrane. The cellular damage induced by PAs and PATDs was qualitatively observed through a Calcium/PI staining assay. As illustrated in Fig. S10, the green fluorescence represented the live cells, and the red fluorescence represented the dead cells. As depicted, with the length of the hydrophilic chain of the PAs and PATDs increased, the cellular toxicity of the compound significantly enhanced, and PATD cationic surfactant exhibited higher cytotoxicity than PAs non-ionic surfactant. Interestingly, most of the dead cells in the results of the Calcium/PI staining assay fell off from the culture dish, suggesting that surfactants could cause damage to the cell and lead to cell shedding. Subsequently, we observed the surface calcium adhesive protein of HUVEC-TIE2-L914F cells through immunofluorescence assay. As illustrated in Fig. 3D and F, the green fluorescence represented the labeled calcium adhesive protein on the cell membrane. With the gradual increase of the hydrophilic chain of the PATDs, the strength of the green fluorescence gradually decreased, indicating that PATDs could strip off membrane proteins, causing the cell to fall off, which demonstrated a positive effect in the treatment of vascular sclerotherapy. Finally, we performed a microscopic observation of HUVEC-TIE2-L914F cells treated with PATDs through biological cryogenic scanning electron microscopy. As illustrated in Fig. 3G, the normal HUVEC-TIE2-L914F cell surface was intact with high expression of extracellular vesicles, indicating normal cell function. However, after treatment with PATDs, the cell surface exhibited a large number of pores, and the number of cell surface pores increased with the increase of the hydrophilic chain of the PATDs. This result suggested that the PATDs puncturing of the cell membrane led to cell necrosis. Moreover, the expression of extracellular vesicles on the cell surface disappeared after PATD treatment, indicating that PATDs could strip off surface membrane proteins and ultimately lead to functional loss in cells.

3.5. *Investigation of in vitro PLA-MMPs system inhibition*

Firstly, we investigated the degradation and release rate of TA from PATDs in serum solution. As shown in Fig. 3H, with an increase in hydrophilic chain length, the degradation and release rate of the TA from PATDs increased, and PATD15 exhibited the highest degradation and release rate, with complete degradation occurring within approximately 10 min. This indicated that an increase in hydrophilic chain length favored contact between ester bonds and the active site of the esterase. In addition, we also investigated the effects of TA on the PLA-MMPs system. The results depicted in Fig. 3I showed that when PLA was added to the proMMPs solution, it activated the conversion of proMMPs to MMPs. However, after co-treatment with PLA and TA released from PATDs, the ability of PLA to activate the conversion of proMMPs to MMPs decreased significantly. Among all PATDs, PATD15 exhibited the fastest degradation and release rate of TA and the strongest inhibitory effect on the PLA-MMPs system. Based on the above results, it could be inferred that the inhibitory effect of TA on PLA was beneficial for the

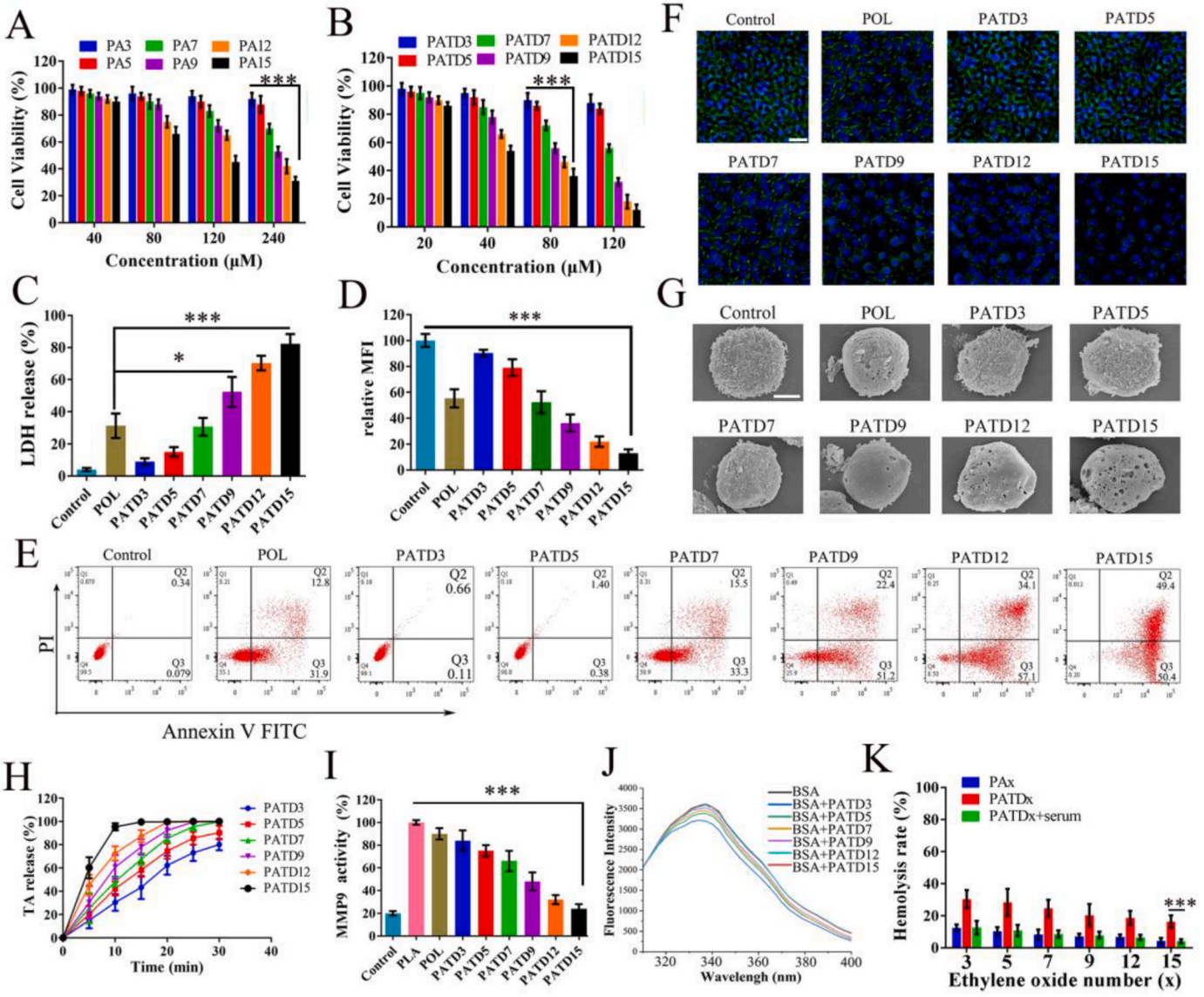

Fig. 3. (A) and (B) *In vitro* cytotoxicity of PAs and PATDs against HUVEC-TIE2-L914F cells for 12 h. (C) LDH release of HUVEC-TIE2-L914F cells treated with 120 μM POL or PATDs for 12 h. (E) Cell apoptosis was detected in HUVEC-TIE2-L914F cells treated with 120 μM PATDs for 12 h by flow cytometry. (D) and (F) Immunofluorescence staining images and mean fluorescent intensity (MFI) of cadherin on HUVEC-TIE2-L914F cells, scale bar = 50 μm. (G) Biological scanning electron microscope image of HUVEC-TIE2-L914F cells treated with 120 μM PATDs for 12 h, scale bar = 5 μm. (H) TA release rate of PATDs in 10 % serum solution. (I) MMP9 inhibition by the degradation product of PATDs. (J) Fluorescence spectrum for BSA protein (0.1 mg mL^{-1}) incubated with PATDs. (K) Hemolysis assay of 0.01 % PAs, PATDs, and PATDs treated with 10 % serum for 15 min, x = the ethylene oxide number of the PA or PATD hydrophilic chain.

inhibition of MMPs activity to reduce the degradation of MMPs on collagen, which was beneficial for the development of tissue fibrosis.

3.6. Investigation of the safety of PATDs in blood

We investigated the blood safety of PATDs by fluorescence testing for their effects on albumin. The results in Fig. 3J showed that when the hydrophilic chain of the PATDs was short, their hydrophobicity was strong, and they had a strong damaging effect on albumin structure. However, as the hydrophilic chain of the PATDs increased gradually, their damaging effect on the albumin structure decreased. Next, we investigated the in vitro hemolytic properties of PAs and PATDs, with results shown in Fig. 3K and S11. The hemolytic effect of PATD cationic surfactant was also stronger than that of PA non-ionic surfactant. However, after incubation with serum, PATDs were degraded by esterase in the serum into non-ionic surfactant and TA, leading to a significant decrease in hemolytic activity. The degradability of the vascular sclerosant and dilution in the blood ensured its safety in situ after administration.

3.7. In vivo retention of hydrogel in the tail vain

The tail vein of 8-week-old Kunming mice was selected as a vascular model for investigating in vivo retention in the vein. A GA solution containing CY7 dye along with a series of PATDs was injected to investigate the retention of gel in the tail vein. As depicted in Fig. S12, the injection of the GA solution containing only CY7 dye exhibited minimal retention within the blood vessels. On the other hand, the injection of the GA solution containing PATD5 did not result in the formation of a stable gel, leading to its rapid dissolution within about 15 min. However, the GA solution containing PATD9 formed a relatively stable gel and demonstrated retention for up to 60 min before dissolution. Furthermore, the gel formed by PATD15 showed greater stability and exhibited prolonged retention, persisting for more than 120 min

before ultimately dissolving. From the above results, it was clear that the gel formed by PATD15 exhibited the longest duration of retention within the blood vessels, ultimately dissolving gradually, thereby mitigating any potential immune rejection caused by gel retention. Next, we examined the flow of blood within the blood vessels using Doppler color ultrasound imaging, as shown in Fig. 4A. In the control group, three flowing blood vessels were observed, consisting of an upper arterial vessel and two lower venous vessels. Following 30 min of administration of TA, PA5/GA, and PATD5/GA, no impact on blood flow was observed, indicating that these drug formulations were unable to form stable gels and achieve vascular retention. Conversely, after administration of PA9/GA, PATD9/GA, PA15/GA, and PATD15/GA, a reduction in the diameter of the venous blood vessels was observed, implying that these drug formulations were capable of forming gels within the veins and achieving vascular retention.

3.8. Investigation of in vivo PLA-MMPs system inhibition

The PLA levels and MMPs activity in the blood of mice after administration of the PATDs/GA were measured, as depicted in Fig. 4B. In the TA, PA5/GA, and PATD5/GA groups, there was little change in PLA levels, which could be attributed to the minimal damage to endothelial cells caused by these drug administrations. Consequently, there was no initiation of the clotting-fibrinolysis cascade reaction. However, in the PA9/GA, PATD9/GA, PA15/GA, and PATD15/GA groups, there was a significant increase in PLA levels, indicating the destruction of

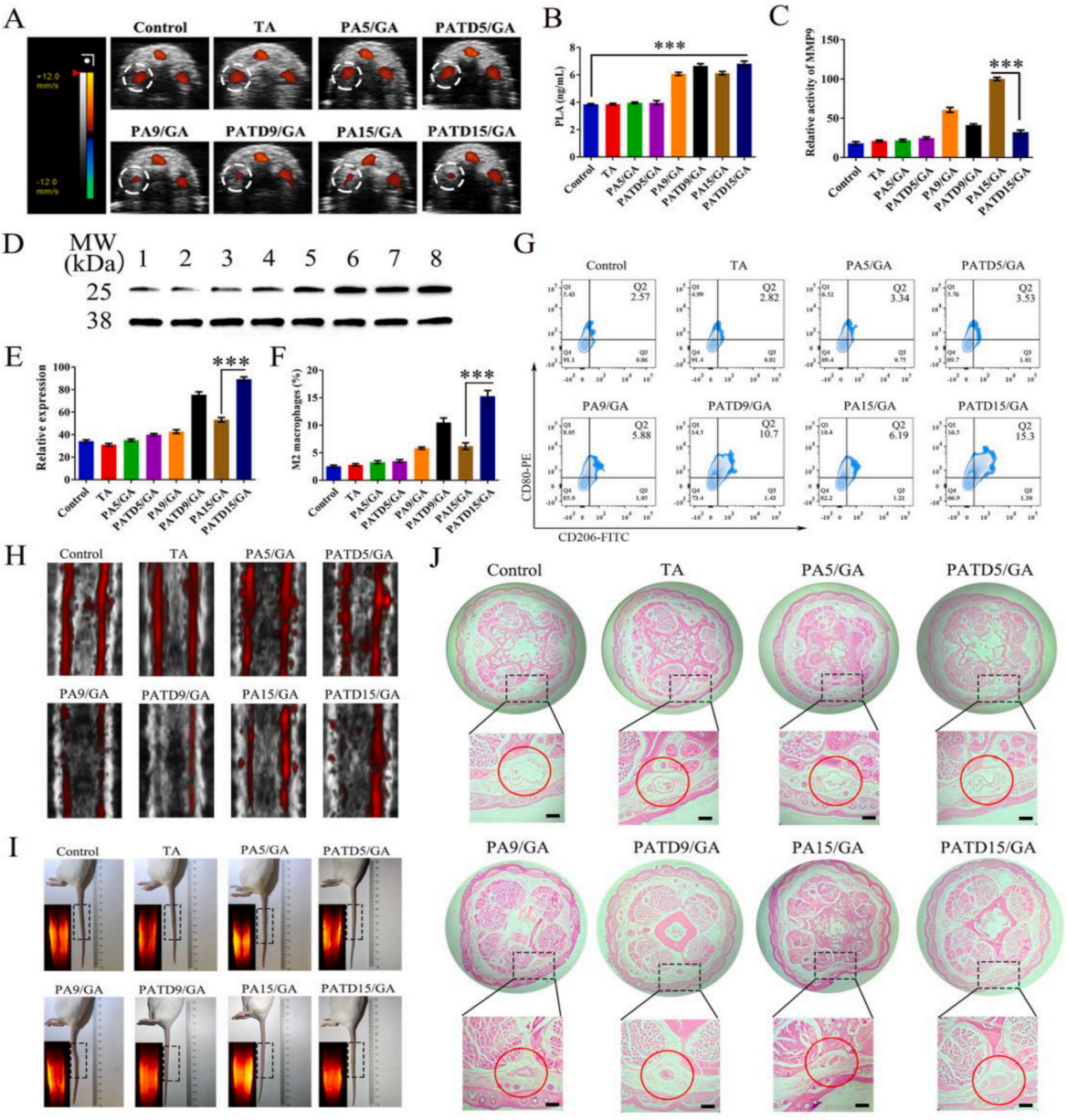

Fig. 4. (A) 2D Doppler ultrasound images of mice tail after treatment at 30 min. (B) PLA level in the blood after treatment with saline, PAs/GA and PATDs/GA respectively at 24 h. (C) Relative MMP9 activity in the blood after treatment with saline, PAs/GA and PATDs/GA respectively at 24 h. (D) and (E) Protein levels of TGF-β1 in tail tissues after treatments at 3rd day determined by Western blot (1.Control, 2.TA, 3. PA5/GA, 4.PATD5/GA, 5.PA9/GA, 6.PATD9/GA, 7.PA15/GA, 8. PATD15/GA) and cumulative densitometric analyses of the TGF-β1 bands were performed by Image J. (F) and (G) Flow cytometric analyses of M2 macrophages in tail tissues after treatments at 3rd day and populations of $CD80^{+}CD206^{+}$ cells. (H) Representative 3D US/PA images of in vivo tail tissues on the 7th day. (I) Photos of the tail veins of Kunming mice after treatment with saline, PAs/GA and PATDs/GA on the 7th day. The embedded pictures are the tail vein vessels under 0.5 W yellow LED light. (J) H&E staining of the tail veins of Kunming mice treated with saline, PAs/GA and PATDs/GA respectively on the 7th day, scale bar = 100 μm.

endothelial cells by these drugs and subsequent initiation of the clotting-fibrinolysis cascade reaction. From Fig. 4C, it was evident that the MMPs activity remained low in the control, TA, PA5/GA, and PATD5/GA groups. However, after treatment with PA9/GA and PA15/GA, there was a marked activation of MMPs activity. In the PATD9/GA and PATD15/GA groups, the activation of MMPs was not significant. It could be inferred from these findings that the degradation and release of TA by PATD9 and PATD15 inhibited the activity of the PLA-MMPs system. MMPs not only degraded collagen, which was necessary for tissue fibrosis but also impacted the expression of signaling proteins involved in the process of tissue fibrosis. In order to further investigate the impact of PATDs on the inhibition of the PLA-MMPs system in tissue fibrosis processes, we assessed the levels of TGF-β1, an important fibrosis-related signaling protein, in mouse tail tissues using Western blot analysis. The results, shown in Fig. 4D and E, in the PA9/GA, PATD9/GA, PA15/GA, and PATD15/GA groups, there was a significant upregulation in the expression of TGF-β1. Among these groups, the highest expression of TGF-β1 was observed in PATD9/GA and PATD15/GA groups, which contained TA. Therefore, it could be inferred from the aforementioned results that TA released from PATD9 and PATD15 inhibited the PLA-MMPs, thereby facilitating the expression of fibrosis-related signaling proteins. Additionally, we determined the levels of M2 macrophages ($CD80^{+}CD206^{+}$ cells), which were immune cells associated with tissue fibrosis, in mouse tail tissues using flow cytometry (Fig. 4F and G). Similarly, in the PA9/GA, PATD9/GA, PA15/GA, and PATD15/GA groups, there was a significant upregulation in the expression of M2 macrophages. Among these groups, the highest levels of M2 macrophages were observed in PATD9/GA and PATD15/GA groups, indicating that TA released from PATD9 and PATD15 inhibited the PLA-MMPs system, promoting polarization of macrophages towards the M2 phenotype. An increase in the number of M2 macrophages would contribute to tissue fibrosis and scar formation.

3.9. Evaluation of embolus in mouse tail vein

To assess the therapeutic effect of PAs/GA and PATDs/GA administered via in-site gel formulation in a mouse tail vein model, we employed photoacoustic imaging to observe the blood vessels after 7 days of treatment. The results were shown in Fig. 4H. The background of the image represented the 2D ultrasound mode image of the mouse tail tissue, while the red fluorescence represented the images of two vein blood vessels. The left vein blood vessel corresponded to the drug-administered vessel. From the results, it could be observed that the TA, PA5/GA, and PATD5/GA groups exhibited intact vein blood vessels similar to the control group, indicating that these drugs did not induce vascular damage. In contrast, the PA9/GA group showed a slight thinning of the left administered blood vessel, suggesting poor drug efficacy as the vessel did not completely disappear. The PATD9/GA group, on the other hand, displayed a significant reduction in the left administered blood vessel, indicating the enhanced vascular sclerosing effect of PATD cationic surfactant. Furthermore, in both the PA9/GA and PATD9/GA groups, the right vein blood vessels also displayed vessel narrowing, which might be attributed to the poor gel stability of the PA9/GA and PATD9/GA groups during initial drug administration. The diffusion of the drug with GA could have damaged the adjacent non-administered blood vessels. In the PA15/GA group, the left administered blood vessel exhibited thinning, demonstrating that the non-ionic surfactant in PA15 caused minimal endothelial cell damage without completely obliterating the blood vessel. Conversely, in the PATD15/GA group, the left administered blood vessel significantly disappeared, indicating that the cationic surfactant PATD15 enhances vascular injury, resulting in complete vessel disappearance. In both the PA15/GA and PATD15/GA groups, the right non-administered blood vessels remained intact, indicating that the high gel stability of PA15 and PATD15 reduced their diffusion during initial administration with GA, thereby almost completely avoiding diffusing into the non-administered blood vessels. Additionally, we performed direct observation of the mouse tail vein subjected to drug administration using a yellow LED light. The results shown in Fig. 4I revealed that blood vessels in the control group had a black linear appearance under LED illumination. In the PA15/GA group, relatively thin blood vessels could still be observed, while in the PATD15/GA group, the blood vessels were virtually completely absent, indicating a stronger effect of PATD15 cationic surfactant. Finally, we conducted H&E staining of the administered mouse tail tissues (Fig. 4J). The results indicated that in the control, TA, PA5/GA, and PATD5/GA groups, the administered blood vessels still appeared as intact hollow structures, suggesting the absence of vascular damage caused by these drugs. In the PA9/GA and PA15/GA groups, the blood vessel walls appeared thicker and the vessels narrower, but they were not completely occluded. In the PATD9/GA group, the blood vessel walls were thicker, and significant vessel constriction was observed. In the PATD15/GA group, the central region of the blood vessel was filled with tissue, nearly completely undergoing sclerosis. Considering all the experimental results, it was evident that PATD15 exhibited the most significant effect on vascular sclerosis. Additionally, the PATD15 in-site gel showed high retention at the administration site, reducing the risk of ectopic vessel damage.

3.10. Evaluation of embolus in rabbit ear marginal vein

To further investigate the therapeutic effect of cationic surfactants based on vascular damage and PLA system inhibition in treating venous malformation, we selected the PATD15/GA with the best sclerosing effect in the mouse tail vein vascular model and its control group PA15/GA to conduct further pharmacological testing in the rabbit ear marginal vein with thicker blood vessels. We selected rabbits weighing 2 kg for drug administration and took pictures before administration, on the 1st, 3rd, 7th, 14th, 18th, and 21st day for observation. The results were shown in Fig. 5A. The TA group and control group had no changes in vascular status within 21 days, indicating that pure TA would not cause coagulation reactions and had no damaging effects on blood vessels. The PA15/GA and PATD15/GA administration groups had blackened blood vessels from the first day to the third day, and vascular hardening began to gradually disappear by the 7th day. By the 21st day, only a small portion of the vessel in the PA15/GA administration group had disappeared, about 6 cm, and the rest could still be seen with thinner blood vessels, suggesting the presence of neovascularization. The vessel in the PATD15/GA administration group had almost completely disappeared, with the length of the disappeared blood vessels being up to 18 cm. To investigate the extent of damage to the blood vessels by PA15 and PATD15, we chose the rabbit ear tissue administered after 24 h for immunofluorescence observation. The intima membranes of blood vessels were marked by CD31 antibody (red), and the medial membranes of blood vessels were marked by α-actin (green). The results (Fig. 5C) showed that in the control and TA groups, intima and media membranes of the blood vessel had strong red and green fluorescence intensity, while in the PA15/GA group, the red fluorescence intensity of blood vessels decreased significantly, while the green fluorescence intensity decreased slightly, indicating that the nonionic surfactant PA15 caused weaker damage to the blood vessel and could not cause serious damage to the media membranes. In contrast, the red and green fluorescence intensity of blood vessels in the PATD15/GA group decreased significantly, indicating that the cationic surfactant-based PATD15 caused stronger damage to the blood vessels, affecting both the intima and media membranes. Next, through the detection of circulating endothelial cells (CECs), it could be seen that the CECs in the PATD15/GA group were significantly more than those in the PA15/GA group (Fig. 5F), indicating that the blood vessel damage caused by the cationic surfactant-based PATD15 was stronger than that of the PA15, causing more endothelial cells to fall off into the bloodstream.

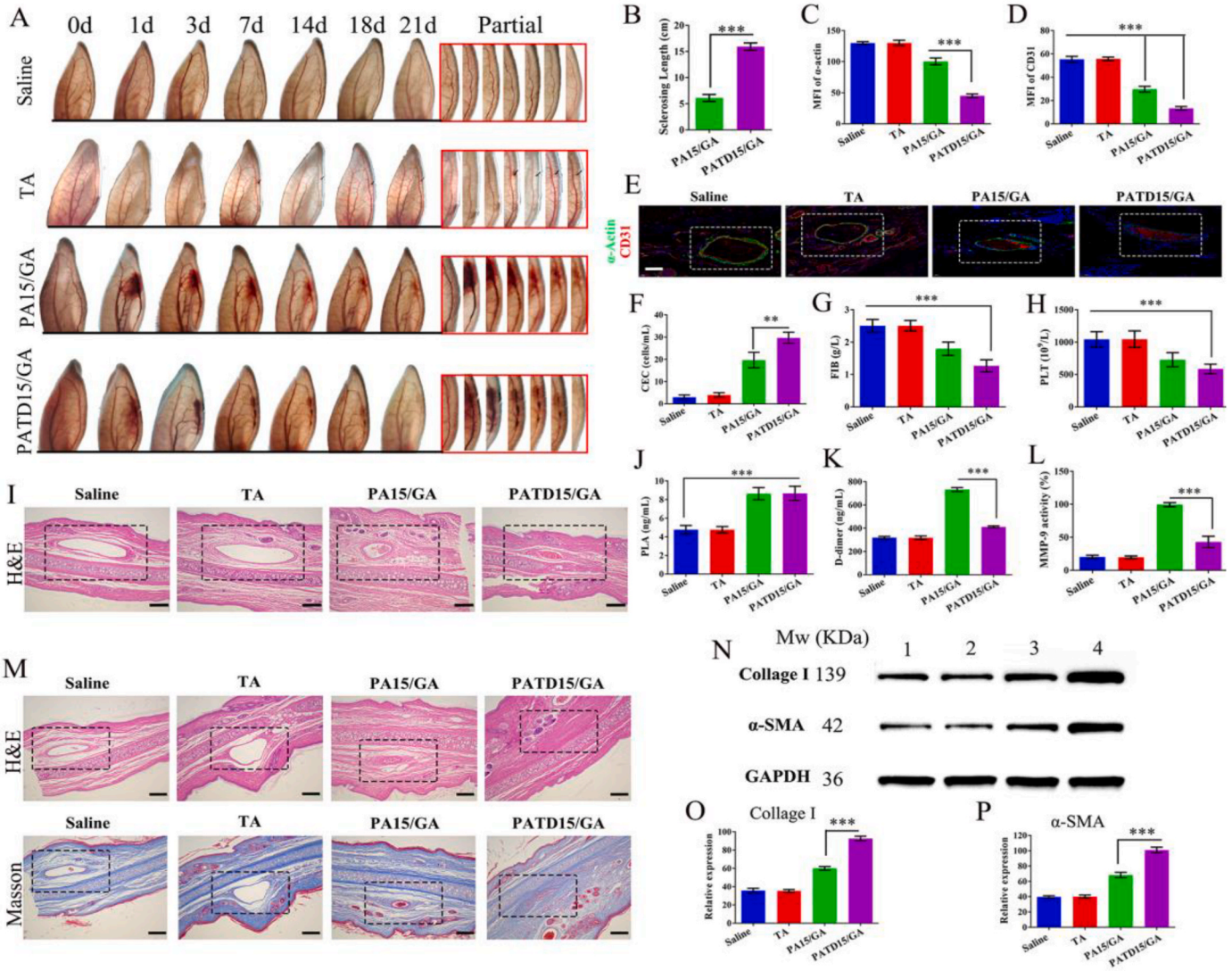

Fig. 5. (A) Sclerotherapy study on rabbit ear marginal vein treated with TA, PA15/GA, PATD15/GA for 21 days, respectively. (B) Sclerosing length of rabbit ear marginal vein after different treatments on the 21st day. (C), (D), and (E) Immunofluorescence staining images and mean fluorescent intensity (MFI) of CD31 and α-actin in rabbit ear marginal vein after different treatments at 24 h, scale bar = 100 μm. (F) Quantitation of circulating endothelial cells (CECs) in the blood after treatment with saline, TA, PA15/GA, PATD15/GA at 24 h. (G) and (H) Quantitation of fibrin (FIB) and platelets (PLT) in the blood after treatments on the 3rd day. (I) H&E staining of rabbit ear marginal vein after different treatments on the 3rd day, scale bar = 100 μm. (J) Quantitation of PLA in the blood after treatments on the 3rd day. (K) Quantitation of D-dimer in the blood after treatments on the 3rd day. (L) Relative MMP9 activity in the blood after treatments on the 3rd day. (M) H&E staining and Masson analysis of rabbit ear marginal vein after different treatments on the 21st day, scale bar = 100 μm. (N), (O), and (P) Expression of collagen I (139 kDa) and α-SMA (42 kDa) in rabbit ear, determined by Western blotting (1.Control, 2.TA, 3.PA15/GA, 4.PATD15/GA). GAPDH was used as an internal reference.

3.11. Investigation of in vivo PLA-MMPs system inhibition

For further investigation of the clotting of blood after blood vessel damage, we took blood samples from the rabbits administered on the third day to determine the levels of fibrin and platelets related to blood coagulation. The results showed that the levels of fibrin and platelets in both the PA15/GA and PATD15/GA groups decreased, indicating the formation of thrombosis (Fig. 5G and H). Next, we took rabbit ear tissue administered on the third day for H&E staining observation (Fig. 5I). The central part of the blood vessel in the PA15/GA group had thrombus formation, but the thrombus did not fill the entire blood vessel, while in the PATD15/GA group, the blood vessel was completely filled with thrombus. The results of PLA content measurement (Fig. 5J) showed that the PLA concentration in the blood was increased after PA15/GA and PATD15/GA treatment. It could be inferred that the formation of thrombosis after sclerosant treatment activated the PLA, which might induce the risk of ectopic embolism caused by the fragments generated from thrombus degradation. The D-dimer is a fragment resulting from the degradation of a blood clot by PLA and it serves as an indicator of clot degradation. As shown in Fig. 5K, it could be seen that the D-dimer levels in the PA15/GA group were significantly higher than in the PATD15/GA group. This suggested that the release of the TA by PATD15 inhibited the PLA from degrading the blood clot, thereby reducing the risk of ectopic embolism caused by fragments generated during blood clot degradation. We further determined the MMPs activity to investigate the effect of TA released from PATDs on the PLA-MMPs system. The results showed that the MMPs activities of both the PA15/GA and PATD15/GA groups were upregulated to a certain extent after blood vessel damage (Fig. 5L). The MMPs activity of the PATD15/GA group was significantly lower than that of the PA15/GA group, indicating that the degradation release of TA in PATD15 could inhibit the activity of the PLA-MMPs system. Through ELISA analysis of the levels of signal proteins TGF-β, CTGF, and bFGF that were important for vascular fibrosis in blood samples collected on the 7th day after administration (Fig. S13),

the results showed that both the PA15/GA and PATD15/GA groups expressed fibrosis-related signal proteins, and the expression levels of fibrosis-related signal proteins in the PATD15/GA group were significantly higher than those in the PA15/GA group. This indicated that the vascular damage based on cationic surfactants and the PLA inhibition could significantly promote the process of vascular fibrosis.

3.12. Investigation of PATDs vascular sclerosis mechanism in vivo

In order to evaluate the degree of vascular fibrosis after treatment with PAs and PATDs, we performed H&E staining on rabbit ear tissues harvested on the 21st day after drug administration. The results were shown in Fig. 5M. In the PA15/GA group, incomplete occlusion of the central vessels could still be observed on the 21st day after treatment, with some small newly formed blood vessels around the administered venous vessels. In contrast, in the PATD15/GA group, the vessels were almost completely occluded after 21 days of treatment. Subsequently, we analyzed the composition of the occluded vessels using Masson's trichrome staining. The results were shown in Fig. 5M, the blue color represented collagen tissue and the red color represented muscle fiber tissue. In the occluded vessels of the PATD15/GA group, a substantial amount of blue collagen fibers and a small amount of red muscle fiber tissue were present. This indicated that after PATD15 treatment, the vessels were primarily filled with collagen fibers, which promoted the proliferation and differentiation of fibroblasts, while a small amount of muscle fiber tissue helped in the contraction and closure of damaged vessels. Furthermore, we performed Western blot analysis on the rabbit ear tissues harvested on the 21st day after drug administration. The results showed in Fig. 5N, O, and P revealed a significant upregulation of the 139 kDa collagen protein expression in the PATD15/GA group. This finding was consistent with Masson's trichrome staining results and suggested that the degradation and release of TA from PATD15 inhibited the PLA-MMPs system, promoting collagen deposition and providing conditions for tissue fibrosis. The 42 kDa α-SMA protein, a marker for fibroblasts, was highly expressed in the PATD15/GA group, indicating that the occluded vessels were filled with fibroblasts. This was attributed to the deposition of collagen, which provided a growth environment for fibroblast proliferation and differentiation.

To evaluate the in vivo safety of PATD15, we assessed the liver and kidney functions. Fig. S14 revealed that the representative blood biochemical analysis parameters of liver functions parameters (ALT, γ-GT, ALB) and kidney functions parameters (BUN, UA) in the drug-treated groups were consistent with those in the saline group, indicating that the formulation did not affect the liver and kidney functions of the rabbits. Finally, we performed H&E staining analysis on the main organs of the rabbits harvested on the 21st day after drug administration (Fig. S15). The results showed that both PA15 and PATD15 did not cause any damage to the major organs, demonstrating the safety of their administration.

4. Discussion

Currently, commonly used surfactant-based sclerosing agents in clinical practice include POL and STS, which belong to non-ionic surfactants and anionic surfactants, respectively. However, their therapeutic effects are not ideal. Whiteley and coworkers have demonstrated that the degree of damage caused by surfactants to blood vessels has a significant impact on their sclerosing effects [30,31]. Among them, POL can only cause damage to the intimal layer of the blood vessels, while STS can cause certain damage to both the intimal and medial layers. Consequently, the sclerosing effect of STS is stronger than that of POL, but it still fails to completely sclerose the blood vessels. To address this issue, we constructed a more cytotoxic cationic surfactant by linking non-ionic surfactant PAs and TA through ester bonds. As expected, this cationic surfactant can cause stronger damage to both the intimal and medial layers of the blood vessels, while the degradability of the ester bonds ensures its safety for in vivo applications. The TA released from PATDs degradation can promote the process of fibrosis in blood vessels, mainly by inhibiting the activity of the PLA-MMPs system, thereby facilitating the expression of collagen required for fibrosis. This result is consistent with previous research, where using doxycycline inhibited the activity of MMPs, promoting the fibrosis process in blood vessels [16]. Additionally, this study used a mixture of PATDs and GA as a low molecular weight in situ gel for drug delivery. Compared to previously clinically used in situ gels such as ethyl cellulose or corn zein [32,33], the erosion rate of the PATDs/GA in situ gel is faster, completely eroding within 2 h. This could avoid the risk of immune rejection reactions caused by prolonged retention of the gel. This study provides a new idea for the design of novel sclerosing agents and their drug delivery systems.

5. Conclusion

In order to develop an efficient and biocompatible vascular sclerosis agent and its in-site gel-based drug delivery system, this study selected six kinds of PAs composed of twelve straight-chain alkanes as hydrophobic chains and the hydrophilic chains consisting of varying numbers of ethylene oxide polymeric units. The hydroxyl groups at the end of the hydrophilic chains of PAs and the carboxyl groups of TA were connected through ester bonds to synthesize the PATDs with increasing lengths of hydrophilic chains. Through rheological properties examination of the gel, in vitro cytotoxicity experiments, in vitro PLA-MMPs activity inhibition experiments, and in vivo treatment of vascular sclerosis in mouse tail vein experiments, the vascular sclerosis agent with the optimal treatment effect was selected. The results indicated that PATD15 had the optimal hydrophilic/hydrophobic chain ratio. Its cationic surfactant properties could cause the greatest damage to negatively charged endothelial cells, causing them to detach from the blood vessels, exposing the collagen tissues, and activating the PLA system. The ester bonds in the PATD15 could be rapidly degraded by esterases in the blood, releasing the TA to inhibit the activity of PLA and inhibit the conversion of proMMPs to MMPs by PLA. This could promote collagen deposition and fibroblast proliferation and differentiation required for tissue fibrosis, ultimately leading to the complete disappearance of the treated blood vessels. Furthermore, due to the presence of both hydrophobic long chains and hydrophilic long chains in the PATD15 molecule, it could form an in-situ gel in aqueous solutions, allowing the drug to remain in the diseased blood vessels for approximately 120 min, greatly improving its retention. At the same time, this low-molecular-weight gel could spontaneously dissolve, avoiding immune rejection caused by long-term retention of gel formulations in blood vessels. The easy degradability of the ester bonds in PATD15 significantly reduced the risk of systemic toxicity. Therefore, the dual action mechanism of PATDs and their in-situ gel drug delivery system provided an important theoretical basis for the development of novel vascular sclerosis agents.

CRediT authorship contribution statement

Pingtian Ding, Xinggang Yang, Keda Zhang, Xiaoyun Zhao, and Jizhuang Ma designed the research. Jizhuang Ma and Yu Ding carried out the experiments. Yongfeng Chen and Huichao Xie performed data analysis. Wenhan Li and Di Song participated in some of the experiments. Haoran Niu and Bao Li provided experimental drugs and quality control. Jizhuang Ma, and Tianzhi Yang wrote the manuscript. Tong Yu and Xiaoyu Huang revised the manuscript.

Funding

Special projects in key areas of ordinary universities in Guangdong Province (2023ZDZX2054), Natural Science Foundation of Top Talent of SZTU (GDRC202305), Basic Scientific Research Funding of Education Department of Liaoning Province (JYTMS20231368) .

Declaration of competing interest

The authors declare that they have no known competing financial interests or personal relationships that could have appeared to influence the work reported in this paper.

Appendix A. Supplementary data

Supplementary data to this article can be found online at https://doi.org/10.1016/j.mtbio.2024.101376.

Data availability

The data that has been used is confidential.

References

[1] A.N. Hage, J.F.B. Chick, R.N. Srinivasa, J.J. Bundy, N.R. Chauhan, M. Acord, J. J. Gemmete, Treatment of venous malformations: the data, where we are, and how it is done, Tech. Vasc. Intervent. Radiol. 21 (2) (2018) 45–54.

[2] A.K. Greene, A.I. Alomari, Management of venous malformations, Clin. Plast. Surg. 38 (1) (2011) 83–93.

[3] Y.Y. Han, L.M. Sun, S.M. Yuan, Localized intravascular coagulation in venous malformations: a system review, Phlebology 36 (1) (2021) 38–42.

[4] R. Dasgupta, M. Patel, Venous malformations, Semin. Pediatr. Surg. 23 (4) (2014) 198–202.

[5] S. Behravesh, W. Yakes, N. Gupta, S. Naidu, B.W. Chong, A. Khademhosseini, R. Oklu, Venous malformations: clinical diagnosis and treatment, Cardiovasc. Diagn. Ther. 6 (6) (2016) 557–569.

[6] E. Rabe, F. Pannier, Sclerotherapy in venous malformation, Phlebology 28 (2013) 188–191.

[7] S. Ali, S.E. Mitchell, Outcomes of venous malformation sclerotherapy: a review of study methodology and long-term results, Semin. Intervent. Radiol. 34 (3) (2017) 288–293.

[8] D.M. Eckmann, Polidocanol for endovenous microfoam sclerosant therapy, Expet Opin. Invest. Drugs 18 (12) (2009) 1919–1927.

[9] A. Cavezzi, K. Parsi, Complications of foam sclerotherapy, Phlebology 27 (2012) 46–51.

[10] R. Loffroy, B. Guiu, J.P. Cercueil, D. Krausé, Endovascular therapeutic embolisation: an overview of occluding agents and their effects on embolised tissues, Curr. Vasc. Pharmacol. 7 (2) (2009) 250–263.

[11] Y.H. Jiang, J.C. Liu, J.B. Qin, J.H. Lei, X. Zhang, Z.J. Xu, W.M. Li, X.B. Liu, R. H. Wang, B. Li, X.W. Lu, Light-activated gold nanorods for effective therapy of venous malformation, Mater. Today Bio 16 (2022) 100401.

[12] K. Cullion, L.C. Petishnok, H. Koo, B. Harty, J.M. Melero-Martin, D.S. Kohane, Targeting nanoparticles to bioengineered human vascular networks, Nano Lett. 21 (15) (2021) 6609–6616.

[13] X.S. Li, J.F. Lovell, J. Yoon, X.Y. Chen, Clinical development and potential of photothermal and photodynamic therapies for cancer, Nat. Rev. Clin. Oncol. 17 (11) (2020) 657–674.

[14] F. Zehtabi, A. Gangrade, K. Tseng, R. Haghniaz, R. Abbasgholizadeh, H. Montazerian, D. Khorsandi, J. Bahari, A. Ahari, N. Mohaghegh, N. H. Kouchehbaghi, K. Mandal, M. Mecwan, A. Rashad, N.R. de Barros, Y. Byun, M. Ermis, H.J. Kim, A. Khademhosseini, Injectable shear-thinning hydrogels with sclerosing and matrix metalloproteinase modulatory properties for the treatment of vascular malformations, Adv. Funct. Mater. 33 (51) (2023) 2305880.

[15] R.K. Avery, H. Albadawi, M. Akbari, Y.S. Zhang, M.J. Duggan, D.V. Sahani, B. D. Olsen, A. Khademhosseini, R. Oklu, An injectable shear-thinning biomaterial for endovascular embolization, Sci. Transl. Med. 8 (365) (2016) 365ra156.

[16] F. Zehtabi, P. Ispas-Szabo, D. Djerir, L. Sivakumaran, B. Annabi, G. Soulez, M. A. Mateescu, S. Lerouge, Chitosan-doxycycline hydrogel: an MMP inhibitor/sclerosing embolizing agent as a new approach to endoleak prevention and treatment after endovascular aneurysm repair, Acta Biomater. 64 (2017) 94–105.

[17] L. Zhang, F. Chen, J.T. Zheng, H.W. Wang, X.J. Qin, W.S. Pan, Chitosan-based liposomal thermogels for the controlled delivery of pingyangmycin: design, optimization and in vitro and in vivo studies, Drug Deliv. 25 (1) (2018) 690–702.

[18] F. Chen, S.S. Song, H.W. Wang, W.J. Zhang, C.C. Lin, S.L. Ma, T.T. Ye, L. Zhang, X. G. Yang, X.J. Qin, W.S. Pan, Injectable chitosan thermogels for sustained and localized delivery of pingyangmycin in vascular malformations, Int. J. Pharm. 476 (1–2) (2014) 232–240.

[19] S.E.R. Horbach, I.M. Rigter, J.H.S. Smitt, J.A. Reekers, P.I. Spuls, C. van der Horst, Intralesional bleomycin injections for vascular malformations: a systematic review and meta-analysis, Plast. Reconstr. Surg. 137 (1) (2016) 244–256.

[20] M. Kang, A. Yang, P. Hannaford, D. Connor, K. Parsi, Skin necrosis following sclerotherapy. Part 2: risk minimisation and management strategies, Phlebology 37 (9) (2022) 628–643.

[21] J.N. Markovic, U. Nag, C.K. Shortell, Safety and efficacy of foam sclerotherapy for treatment of low-flow vascular malformations in children, J. Vas. Surg.Venous Lymp. Dis. 8 (6) (2020) 1074–1082.

[22] J.Z. Ma, Y.F. Chen, K.D. Zhang, T.Z. Yang, H.C. Xie, X.G. Yang, P.T. Ding, Study of vascular sclerosing agent based on the dual mechanism of vascular endothelial cell damage-plasmin system inhibition, Biochem. Biophys. Res. Commun. 680 (2023) 135–140.

[23] J.B. Jun, M. Kuechle, J.M. Harlan, K.B. Elkon, Fibroblast and endothelial apoptosis in systemic sclerosis, Curr. Opin. Rheumatol. 15 (6) (2003) 756–760.

[24] G.A. Ramirez, S. Franchini, P. Rovere-Querini, M.G. Sabbadini, A.A. Manfredi, N. Maugeri, The role of platelets in the pathogenesis of systemic sclerosis, Front. Immunol. 3 (2012) 160.

[25] K. Parsi, T. Exner, D.E. Connor, D.D.F. Ma, J.E. Joseph, *In vitro* effects of detergent Sclerosants on coagulation, platelets and microparticles, Eur. J. Vasc. Endovasc. Surg. 34 (6) (2007) 731–740.

[26] Y. Kanno, E. Shu, α2-Antiplasmin as a potential therapeutic target for systemic sclerosis, Life-Basel 12 (3) (2022) 396.

[27] P. Star, D.E. Connor, K. Parsi, Novel developments in foam sclerotherapy: focus on Varithena® (polidocanol endovenous microfoam) in the management of varicose veins, Phlebology 33 (3) (2018) 150–162.

[28] V. Nastasa, K. Samaras, C. Ampatzidis, T.D. Karapantsios, M.A. Trelles, J. Moreno-Moraga, A. Smarandache, M.L. Pascu, Properties of polidocanol foam in view of its use in sclerotherapy, Int. J. Pharm. 478 (2) (2015) 588–596.

[29] P.L. McCormack, Tranexamic acid A review of its use in the treatment of hyperfibrinolysis, Drugs 72 (5) (2012) 585–617.

[30] M.S. Whiteley, S.J. Dos Santos, T.J. Fernandez-Hart, C.T.D. Lee, J.M. Li, Media damage following detergent sclerotherapy appears to be secondary to the induction of inflammation and apoptosis: an immunohistochemical study elucidating previous histological observations, Eur. J. Vasc. Endovasc. Surg. 51 (3) (2016) 421–428.

[31] M.S. Whiteley, S.J. Dos Santos, C.T. Lee, J.M. Li, Mechanochemical ablation causes endothelial and medial damage to the vein wall resulting in deeper penetration of sclerosant compared with sclerotherapy alone in extrafascial great saphenous vein using an ex vivo model, J. Vas. Surg.Venous Lymp. Dis. 5 (3) (2017) 370–377.

[32] A. Dompmartin, X. Blaizot, J. Théron, F. Hammer, Y. Chene, D. Labbé, M. T. Barrellier, C. Gaillard, R. Leroyer, V. Chedru, C. Ollivier, M. Vikkula, L.M. Boon, Radio-opaque ethylcellulose-ethanol is a safe and efficient sclerosing agent for venous malformations, Eur. Radiol. 21 (12) (2011) 2647–2656.

[33] K. Sannier, A. Dompmartin, J. Théron, D. Labbé, M.T. Barrellier, R. Leroyer, P. Touré, D. Leroy, A new sclerosing agent in the treatment of venous malformations -: study on 23 cases, Intervent Neuroradiol. 10 (2) (2004) 113–127.